Properties of liquid argon scintillation light emission

Ettore Segreto[*]

Instituto de Física "Gleb Wataghin", Universidade Estadual de Campinas—UNICAMP, Rua Sérgio Buarque de Holanda, No 777, CEP 13083-859 Campinas, São Paulo, Brazil

(Received 14 December 2020; accepted 7 January 2021; published 1 February 2021)

Liquid argon is used as active medium in a variety of neutrino and dark matter experiments thanks to its excellent properties of charge yield and transport and as a scintillator. Liquid argon scintillation photons are emitted in a narrow band of 10 nm centered around 127 nm and with a characteristic time profile made by two components originated by the decay of the lowest lying singlet, $^1\Sigma_u^+$, and triplet states, $^3\Sigma_u^+$, of the excimer Ar_2^* to the dissociative ground state. A model is proposed which takes into account the quenching of the long lived triplet states through the self-interaction with other triplet states or through the interaction with molecular Ar_2^+ ions. The model predicts the time profile of the scintillation signals and its dependence on the intensity of an external electric field and on the density of deposited energy, if the relative abundance of the unquenched fast and slow components is know. The model successfully explains the experimentally observed dependence of the characteristic time of the slow component on the intensity of the applied electric field and the increase of photon yield of liquid argon when doped with small quantities of xenon (at the part per million level). The model also predicts the dependence of the pulse shape parameter, F_{prompt}, for electron and nuclear recoils on the recoil energy and the behavior of the relative light yield of nuclear recoils in liquid argon, $\mathcal{L}_{\text{eff}}$.

DOI: 10.1103/PhysRevD.103.043001

I. INTRODUCTION

Liquid argon (LAr) is a powerful medium to detect ionizing particles and is widely used in neutrino and dark matter experiments since several years [1–6]. LAr scintillation photons are emitted in the vacuum ultraviolet in a 10 nm band centered around 127 nm with a time profile made by two components with very different characteristic decay times, a fast one in the nanosecond range and a slower one in the microsecond range [7]. The relative abundance of the two components depends strongly on the ionizing particle type and allows for a powerful particle discrimination [8,9].

LAr based neutrino detectors use the technique of the time projection chamber (TPC) [1–3], which allows to perform a precise tridimensional and calorimetric reconstruction of the charged particles produced by the interaction, through the detection of the scintillation light and of the ionization charge. The detection of scintillation light is crucial to determine the time, T_0, in which the interaction occurs in LAr and the ionization electrons start to drift toward the anode sensing wires, under the action of an external electric field (typically around 500 V/cm). The coordinate along the drift direction is measured as the product of the drift time and the drift velocity [10] with a resolution better than 1 mm. Its precise knowledge is important to correct for the attenuation of the ionization charge during its propagation and to fiducialize the active volume of the detector.

Scintillation light is also used to perform the calorimetric measurement of the energy deposited by the neutrino interaction, which is complementary to the one performed with the ionization charge and contributes to improve the overall energy resolution of the detector. In fact, at a typical electric field of 500 V/cm, about half of the deposited energy goes into scintillation. The photon detection system of the first module of the DUNE (Deep Underground Neutrino Experiment) far detector, for example, is expected to have an energy resolution comparable to the one obtainable with the TPC (between 15% and 20%) for low energy events (below 30 MeV), which is the relevant region for supernova and solar neutrinos [11].

LAr is used as a target in several experiments for direct dark matter searches [6,12–15], thanks to its exceptional particle discrimination power. These experiments search for recoils of argon nuclei induced by the interaction with the hypothetical WIMPs (weakly interacting massive particles), well motivated dark matter candidates in the framework of the ΛCDM (Lambda cold dark matter) model [16]. WIMPs are electrically neutral particles with a mass of the order of hundreds of times the mass of the proton, whose interactions with ordinary matter are mediated by the weak force, as well as by gravity. A WIMP interaction with an argon atom is expected to produce a

[*]segreto@ifi.unicamp.br

nuclear recoil with a very tiny kinetic energy (of the order of few tens of keV), which is only partially transferred to the electrons of the LAr and is detectable. A large fraction of the recoil energy is lost in elastic collisions of the recoiling argon nucleus with other argon nuclei. In this very low energy region, LAr scintillation light is a powerful tool to discriminate electron recoils produced by β and γ background from genuine nuclear recoils, since the relative abundance of fast and slow scintillation components is very different in the two cases. Pulse shape discrimination in LAr allows for a rejection of electron recoils with respect to nuclear recoils at the 1.5×10^7 level [6]. The combination of underground screening of the detector, choice of materials with ultralow radioactive background, use of underground argon with a reduced content of ^{39}Ar and LAr rejection power will allow to push the sensitivity of the next generation of LAr detectors to WIMP-nucleon interaction cross sections down to 1.2×10^{-47} cm^2 for WIMPs of 1 TeV/c^2 mass [17].

LAr scintillation has been deeply studied by several authors [7,18,19] and a solid understanding of the main mechanisms regulating the production, emission and propagation of scintillation photons has been achieved. However, there are experimental results which can not be easily explained and described by the currently accepted models, as the dependence of the characteristic time of the slow component on the intensity of the electric field applied to LAr and the increase of the LAr photon yield when doped with small quantities of xenon, at the level of few ppm (part per million). These phenomena point to quenching mechanisms involving the excited species which are the precursors of the scintillation photons and which have not been investigated before.

The model proposed in this work takes into account these quenching processes and predicts the shape of the scintillation pulse as a function of the applied electric field and of the density of the energy transferred to the electrons of LAr. In addition to the experimental observations mentioned above, it also allows to explain the dependence of the pulse shape parameter, F_{prompt}, on the energy of the incoming particle. The cases of electron and nuclear recoils are explicitly treated and compared to data. The integral of the scintillation pulse allows to estimate the amount of quenching due to these processes and to predict the behavior of the relative light yield of nuclear recoils in LAr, $\mathcal{L}_{\text{eff}}$, as a function of the recoil energy, which is a quantity of central importance for dark matter experiments to understand the fraction of the deposited energy which is transferred to the electrons of the LAr and can be detected.

II. LAR SCINTILLATION MODEL

The passage of ionizing particles in LAr produces free excitons and electron-hole pairs. The proportion between these two species is assumed to be independent of the ionizing particle type and energy: $N_{\text{ex}}/N_i = 0.21$ [20], where N_{ex} is the abundance of excitons and N_i the abundance of electron-hole pairs. Free excitons and holes are self-trapped within about 1 ps from their production and result into excited, Ar_2^*, or ionized, Ar_2^+, argon dimers. Ar_2^+ recombines with a thermalized electron to form Ar_2^* [18] which in turn decays nonradiatively to the first singlet and triplet excited states $^1\Sigma_u^+$ and $^3\Sigma_u^+$. These two states, whose disexcitation leads to the emission of the scintillation photons, have approximately the same energy with respect to the dissociative ground state, while the lifetimes are very different: in the nanosecond range for $^1\Sigma_u^+$ and in the microsecond range for $^3\Sigma_u^+$ [7].

The scintillation photon yield of LAr depends on the ionizing particle type and on the linear energy transfer (LET) [21]. The highest photon yield is reached by relativistic heavy nuclei, from Ne to La. Low LET light particles (e^-, p) have a slightly reduced photon yield due to the fact that a fraction of the ionization electrons escapes from recombination. Nuclear recoils and α particles also have a reduced photon yield, but the quenching mechanism is different and not fully clarified yet. A biexcitonic interaction in the core of the track has been proposed as a possible explanation [18] and a reasonably good agreement is found for 5.3 MeV α particles, while the model is not accurate in explaining the dependence of the photon yield for nuclear recoils [19] at very low energies ($\sim$ tens of keV). In this case, a better agreement with the available data is obtained when using the Birks law to account for the possible quenching processes involving excitons and excited dimers Ar_2^* [22,23].

Two recent experimental observations can not be easily explained with the current understanding of the LAr scintillation process. The DUNE Collaboration has reported a clear dependence of the lifetime of the triplet state $^3\Sigma_u^+$ of the Ar_2^* dimer on the electric field in which the LAr is immersed [24]. The scintillation light was produced by a sample of cosmic muons crossing one of the prototypes of the dual phase DUNE detector, the 4-ton demonstrator [25]. The light was detected with an array of five 8″ photomultipliers (Hamamatsu R5912-02Mod) coated with a wavelength shifter, TetraPhenyl-Butadiene (TPB) [26], to convert the 127 nm photons to 430 nm and the electric field was varied between 0 and 600 V/cm.

The second experimental evidence is related to the doping of LAr with small concentrations of xenon. It has been reported that adding a few tens of ppm of xenon to LAr has the effect of shifting the wavelength of the triplet component from 127 nm to 174 nm, shortening the signal from few μsec to hundreds of nsec and enhancing the light yield (LY) [9]. The enhancement of LY cannot be explained by an higher quantum efficiency of the wavelength shifter (TPB) for 174 nm than for 127 nm, since it has been measured to be almost the same [27] and should be attributed to an increase of the LAr photon yield.

These two effects point to quenching processes of the triplet states and to an hidden amount of light which has not been described before. The proposed quenching mechanisms for the triplet states are two: one relies on the interaction of two excited dimers Ar_2^* and the other on the interaction of one ionized dimer Ar_2^+ with one excited dimer Ar_2^*:

$$Ar_2^* + Ar_2^* \rightarrow Ar_2^* + 2Ar \quad (1)$$

$$Ar_2^* + Ar_2^+ \rightarrow Ar_2^+ + 2Ar. \quad (2)$$

In the absence of an external electric field, reaction 2 is possible when escaping electrons prevent the complete recombination of the ionization charge and thus only for low LET particles (electrons, muons, protons, …).

It is assumed that only the excited dimers in the triplet state participate to this quenching processes, since the lifetime of the singlet state is too short. The instantaneous variation of the number density of triplet states, N_3, and of the number density of ionized dimers (N^+) can be written as:

$$\frac{dN_3}{dt} = D\nabla^2 N_3 - \lambda_3 N_3 - \sigma^+ v^+ N^+ N_3 - \sigma_3 v_3 N_3^2 \quad (3)$$

$$\frac{dN^+}{dt} = D^+ \nabla^2 N^+ \quad (4)$$

where N_3 and N^+ depend on time and position in space, D and D^+ are the diffusion constants of Ar_2^* and Ar_2^+ respectively, λ_3 is the radiative disexcitation rate of the $^3\Sigma_u^+$ state, σ^+ is the cross section for the process 2, v^+ is the relative velocity between a triplet excimer and a ion, σ_3 is the cross section for process (1) and v_3 is the relative velocity of two Ar_2^*.

In the hypotheses that the diffusion terms can be neglected and that Ar_2^* and Ar_2^+ are uniformly distributed inside a cylinder of radius r_3 along the track, Eqs. (3) and (4) reduce to one, which depends only on time:

$$\frac{dN_3}{dt} = -\lambda_3 N_3 - \sigma^+ v^+ N_0^+ N_3 - \sigma_3 v_3 N_3^2 \quad (5)$$

where N_0^+ is the density of Ar_2^+, which is a constant. The hypotheses of the model will be discussed in Sec. VIII. Equation (5) can be solved analytically and gives:

$$N_3(t) = N_0 \frac{e^{-\lambda_q t}}{1 + q/\lambda_q (1 - e^{-\lambda_q t})} \quad (6)$$

where N_0 is the initial density of triplet states, $\lambda_q = \lambda_3 + k^+$, $k^+ = \sigma^+ v^+ N_0^+$, $q = N_0 \sigma_3 v_3$. The LAr scintillation light signal, that is the probability per unit time that an argon excimer decays radiatively to the ground state, can be written as:

$$l(t) = \frac{\alpha_s}{\tau_s} e^{-\frac{t}{\tau_s}} + \frac{\alpha_3}{\tau_3} \frac{e^{-\frac{t}{\tau_q}}}{1 + q\tau_q (1 - e^{-\frac{t}{\tau_q}})} \quad (7)$$

where α_s is the initial abundance of the singlet states, τ_s is the decay time of the singlet states, α_3 is the initial abundance of triplet states, τ_3 is the unquenched decay time of the triplet states, and $\tau_q = 1/(\lambda_3 + k^+) = 1/\lambda_q$. The part of the scintillation signal originating from triplet decays, depends on the electric field and on the LET thorough τ_q and q. The integral, L, of the light signal $l(t)$ is proportional to the total number of scintillation photons emitted and is given by:

$$L = L_s + L_3 = \alpha_s + \alpha_3 \frac{\ln(1 + q\tau_q)}{q\tau_3} \quad (8)$$

L represents the fraction of photons surviving the quenching processes and is equal to one $(\alpha_s + \alpha_3)$ only when q is zero and $\tau_q = \tau_3$.

III. EXTRACTION OF THE PARAMETERS OF THE MODEL FOR ELECTRON AND NUCLEAR RECOILS

Some of the parameters of Eq. (7) for electron and nuclear recoils have been extracted through a fit procedure of experimental waveforms. The data which have been analyzed were collected during the test described in [8,28]. Within the R&D program of the WArP (WIMP Argon Programme) experiment [5] a 4 liters single phase LAr chamber, observed by seven 2″ photomultipliers (ETL D749U), was exposed to neutron (AmBe) and γ sources. The internal surfaces of the LAr chamber were coated with TPB [29] to down-convert the 127 nm LAr scintillation photons to 430 nm making them detectable by the photomultipliers. After a selection of the events based on the

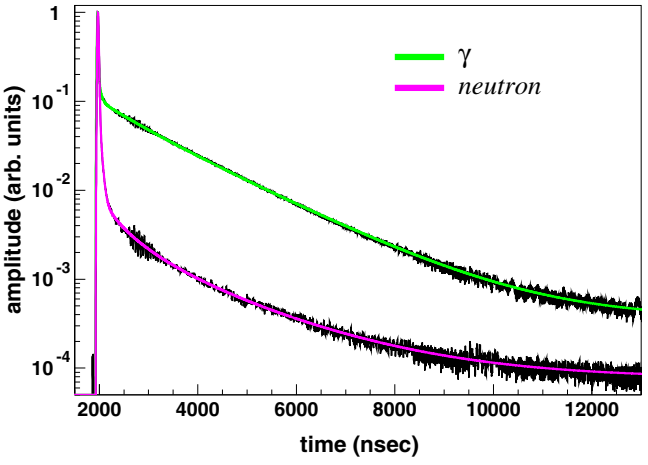

FIG. 1. Average waveforms for gammas and neutrons. Green and magenta lines represent the result of the fitting procedure for gammas and neutrons respectively.

TABLE I. Parameters of the model [Eq. (7)] extracted from the fit procedure. The electron recoil average waveform is constructed with events with a deposited energy between 85 and 100 keV, while the nuclear recoil average waveform with events with a deposited energy between 220 and 290 keV.

	Gamma	Neutron
τ_3 (nsec)	2100 ± 20	
τ_s (nsec)	5 ± 5	
α_s	0.14 ± 0.02	0.64 ± 0.02
f_{TPB}	0.19 ± 0.01	
τ_{TPB} (nsec)	41 ± 5	
α_3	0.86 ± 0.02	0.36 ± 0.02
k^+ (nsec^{-1})	$(1.3 \pm 0.1) \times 10^{-4}$	0.
q (nsec^{-1})	$(2.3 \pm 0.2) \times 10^{-4}$	$(2.3 \pm 0.2) \times 10^{-3}$

shape of the signals, electron and nuclear recoil average waveforms were calculated for different intervals of deposited energy. The LY of the detector was measured to be 1.52 phel/keV for the considered run. An average electron recoil waveform, calculated with signals containing between 130 and 150 phel, and an average nuclear recoil waveform, calculated with signals containing between 150 and 180 phel, have been simultaneously fitted. Considering the LY of the detector these correspond to an energy interval of 85 to 100 keV and of 220 to 290 keV respectively. The fit function contains the amplitudes of the singlet and triplet components (α_s and α_3), the decay time of the singlet component (τ_s), the unquenched decay time of the triplet component (τ_3) and the rate constants k^+ and q. An additional decay component, with decay time of τ_{TPB}, is considered in the fit procedure to take into account the late light reemission of TPB [26]. Its intensity is assumed to be a constant fraction, f_{TPB}, of the fast component, while the remaining fraction, 1-f_{TPB}, is emitted according to the characteristic decay time of the fast scintillation component, τ_s. α_s includes both prompt and delayed TPB fluorescence. The light signal is convoluted with a Gaussian function to accommodate the statistical fluctuations and the response of the read-out electronics.

The parameters which are assumed to be common to the electron and nuclear recoil waveforms are the decay time of the singlet component (τ_s), the unquenched decay time of the triplet component (τ_3) and the fraction of TPB late light, while the other parameters are assumed to be particle dependent. The result of the fit is shown in Fig. 1. The main parameters of the fit are reported in Table I.

IV. DEPENDENCE OF THE SLOW DECAY TIME FROM THE ELECTRIC FIELD AT LOW LET

The shape of the LAr scintillation waveform depends on the module of the applied electric field, $\mathcal{E}$, through the parameters k and q [see Eq. (7)]. The charge recombination factor, $R(\mathcal{E})$, is assumed to have the form:

$$R(E) = B + \frac{A}{1 + k_\mathcal{E}/\mathcal{E}} \tag{9}$$

where B takes into account the fraction of the charge which does not recombine even at null electric field, due to escaping electrons, $k_\mathcal{E}$ is the Birks recombination constant and A is a normalization constant [30].

Equation (9) can be used to make explicit the dependence of the density of Ar_2^+ ions, N_0^+, and of the initial density of triplet states, N_0 on the electric field:

$$N_0^+ = N_i R(\mathcal{E}) \tag{10}$$

$$N_0 = N_i \alpha_3 [1 - R(\mathcal{E}) + N_{ex}/N_i] \tag{11}$$

The parameters k^+ and q can be written as:

$$k^+(\mathcal{E}) = k_0^+ \left[1 + \frac{A}{B(1 + k_\mathcal{E}/\mathcal{E})}\right] \tag{12}$$

$$q(\mathcal{E}) = q_0 \left[1 - \frac{A}{(A + N_{ex}/N_i)(1 + k_\mathcal{E}/\mathcal{E})}\right] \tag{13}$$

where k_0^+ and q_0 are the values of k^+ and q at zero electric field and at a given value of LET. For low LET particles, for which the phenomenon of escaping electrons is present ($k^+ \neq 0$) and when $q\tau_q \ll 1$, the scintillation signal of Eq. (7) presents only a small deviation from a purely exponential decay with a characteristic time of $\tau_{eff} \simeq \tau_q$ and its dependence on the electric field can be explicitly written as:

$$\tau_{eff} \simeq \tau_q = \frac{1}{\frac{1}{\tau_3} + k_0^+ + \frac{k_0^+ A}{B(1+k_\mathcal{E}/\mathcal{E})}} = \frac{1}{\alpha + \frac{\beta}{1+k_\mathcal{E}/\mathcal{E}}} \tag{14}$$

where $\alpha = 1/\tau_{eff}(0)$ is the inverse of the characteristic time at zero electric filed and $\beta = k_0^+ A/B$.

The measurement of the variation of the slow decay time of the LAr scintillation light as a function of the applied electric field, reported in [24], represents, substantially, a measurement of the electron-ion recombination process in LAr performed with light. Experimental points taken from [24] are shown in Fig. 2. They have been fitted with the function of Eq. (14), leaving the parameters α, β and k_E free and the result is shown with a magenta line. The agreement between data and the model is pretty good, with the exception of one of the points at very low electric field. The fit procedure returns a value of $k_\mathcal{E} = 0.075 \pm 0.015$ kV/cm, which is compatible with the value of 0.0486 ± 0.0006 kV/cm $\frac{g/cm^2}{MeV}$ reported in [30], when considering cosmic muons with energies between 1 GeV and 4 GeV and a stopping power between 1.6 $\frac{MeV}{g/cm^2}$ and 2.0 $\frac{MeV}{g/cm^2}$ in LAr.

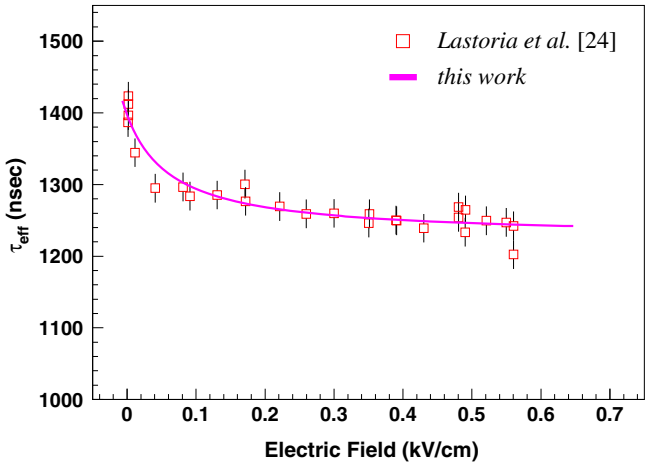

FIG. 2. Variation of the decay time of the slow scintillation component, τ_{eff} as a function of the applied electric field. Magenta line represents a fit of the data with the function of Eq. (14).

V. XENON DOPING OF LAR

It is known that adding xenon to LAr at the level of ppm has the effect of shifting the wavelength of the slow scintillation component from 127 nm to 174 nm [9]. The complete shift of the slow component is observed at tens of ppm of xenon concentration. It has been also reported an increase of the number of detected photons with increasing xenon concentration, which cannot be explained with an increase of the conversion efficiency of the TPB, the wavelength shifter used in the experiment, which has been measured to be almost the same at 127 nm and 174 nm [31].

The mechanism suggested in [32] for the transfer of the excitation energy from argon to xenon can be summarized with the following reaction chain:

$$\text{Ar}_2^* + \text{Xe} \rightarrow (\text{ArXe})^* + \text{Ar} \tag{15}$$

$$(\text{ArXe})^* + \text{Xe} \rightarrow \text{Xe}_2^* + \text{Ar} \tag{16}$$

The energy transfer process and the subsequent emission of 174 nm photons compete with the radiative decay of the Ar_2^* and with the quenching processes described in Sec. II. The net effect is the shift of the slow LAr scintillation component and the partial recovery of the quenched LAr species, which both result in the emission of 174 nm photons with peculiar time characteristics.

In order to understand the gross features of the light emission process from a xenon-argon mixture in the case of low LET particles, it is worth making some rough approximations. For a high enough Xe concentration, it should be possible to neglect second order quenching effects, such as Ar_2^*-Ar_2^*, Ar_2^*-$(\text{ArXe})^*$, $(\text{ArXe})^*$-$(\text{ArXe})^*$. Assuming that the energy transfer between argon and xenon happens without losses and that the reaction rates of the processes $\text{Ar}_2^* + \text{Xe} \rightarrow (\text{ArXe})^*$ and $(\text{ArXe})^* + \text{Xe} \rightarrow \text{Xe}_2^*$ are the same and equal to k_{Xe}, the instantaneous variation of the density of triplet argon states, $N_3^{\text{Ar}}(t)$, of Xe_2^* dimers, $N^{\text{Xe}}(t)$ [33] and of mixed dimers $(\text{ArXe})^*$, $N^{\text{ArXe}}(t)$ can be written as:

$$\frac{dN_3^{\text{Ar}}(t)}{dt} = -\lambda_3 N_3^{\text{Ar}}(t) - k^+ N_3^{\text{Ar}}(t) - k_{\text{Xe}}[\text{Xe}] N_3^{\text{Ar}}(t) \tag{17}$$

$$\frac{dN^{\text{ArXe}}(t)}{dt} = -k_{\text{Xe}}[\text{Xe}] N^{\text{ArXe}}(t) + k_{\text{Xe}}[\text{Xe}] N_3^{\text{Ar}}(t) \tag{18}$$

$$\frac{N^{\text{Xe}}(t)}{dt} = -\lambda_{\text{Xe}} N^{\text{Xe}}(t) + k_{\text{Xe}}[\text{Xe}] N^{\text{ArXe}}(t) \tag{19}$$

where λ_{Xe} is the inverse of the characteristic time of xenon emission and [Xe] is the xenon concentration. Assuming that $\lambda_{\text{Xe}} \gg k_{\text{Xe}}[\text{Xe}]$, Eqs. (17), (18), and (19) can be easily solved with the initial condition that $N^{\text{ArXe}}(0) = 0$ and give the radiative decay probability for the slow LAr scintillation component, $l_3(t)$, and for Xe shifted light, $l_{\text{Xe}}(t)$:

$$l_3(t) = \frac{\alpha_3}{\tau_3} e^{-\frac{t}{\tau_r}} \tag{20}$$

$$l_{\text{Xe}}(t) = \alpha_3 (k_{\text{Xe}}[\text{Xe}])^2 \tau_q [e^{-\frac{t}{\tau_d}} - e^{-\frac{t}{\tau_r}}] \tag{21}$$

where $\tau_r = 1/(k_{\text{Xe}}[\text{Xe}] + 1/\tau_q)$ and $\tau_d = 1/k_{\text{Xe}}[\text{Xe}]$. The radiative decay probability for all the emitted photons, regardless of their wavelength, can be obtained by summing the contributions of Eqs. (20) and (21) to the fast LAr scintillation component, assumed to be unaffected by xenon doping:

$$l(t) = \frac{\alpha_s}{\tau_s} e^{-\frac{t}{\tau_s}} + l_3(t) + l_{\text{Xe}}(t) \tag{22}$$

The total amount of emitted light is obtained by integrating Eq. (22):

$$L = \alpha_s + \alpha_3 \frac{\tau_r}{\tau_3} + \alpha_3 \frac{(k_{\text{Xe}}[\text{Xe}])}{(k_{\text{Xe}}[\text{Xe}]) + 1/\tau_q} \tag{23}$$

Using the parameters of the scintillation waveform for electron recoils found in Sec. III, and the reaction rate $k_{\text{Xe}} = 8.8 \times 10^{-5}$ ppm^{-1} nsec^{-1} (with ppm in mass) reported in [9] it is possible to predict approximately the shape of the scintillation signal for electron recoils and the dependence of the LY on the xenon concentration, [Xe].

Few waveforms for different xenon concentrations are shown in Fig. 3. The exact shape will depend on the precise values of the reaction rates and on the eventual conversion of fast (and slow) LAr scintillation light through photoabsorption by xenon atoms. This would lead to the

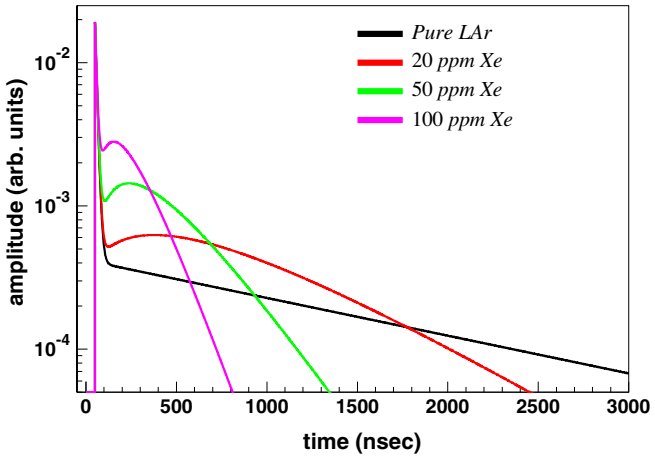

FIG. 3. Waveforms of xenon doped LAr at different xenon concentrations as predicted by the model. The waveforms represent the sum of LAr and xenon shifted light.

formation of $(\mathrm{ArXe})^*$ which would evolve in Xe_2^* according to reaction 16.

The variation of the total LY, which includes 127 nm and 174 nm photons, predicted by the model is shown in Fig. 4 together with the experimental data reported in [9]. There are three different experimental points for each xenon concentration which come from measurements with different gamma sources: the 122 keV photopeak from ^{57}Co, the 511 keV photopeak from ^{22}Na and the 662 keV photopeak from ^{137}Cs. Both model prediction and data have been normalized by their value at zero xenon concentration. An increase of the overall LY around 25% for concentrations above few tens of ppm in mass is observed in the data and correctly predicted by the model. It is reasonable

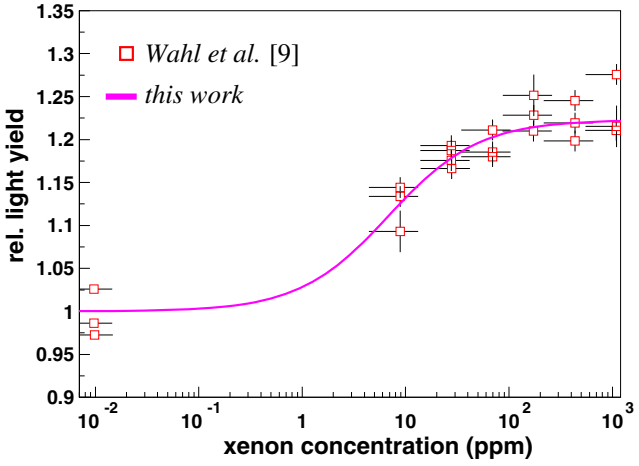

FIG. 4. Variation of the LY of LAr and xenon shifted photons as a function of the xenon concentration in ppm (mass). The experimental points at zero xenon concentration have been shifted to 10^{-2} ppm to facilitate the visualization. The model prediction is shown as a magenta line.

to conclude that the two main approximations made: neglecting second order quenching effects and assuming a lossless transfer of energy between xenon and argon are small and compensate with each other, leading to a good description of the experimental data. The first approximation would lead to an increase of LY, since the amount of quenched Ar_2^* would be higher, while the second would lead to a decrease of LY, because of possible nonradiative disexcitations of the $(\mathrm{ArXe})^*$ states.

VI. F-PROMPT FOR ELECTRON AND NUCLEAR RECOILS

LAr allows for a powerful particle discrimination based on the shape of its scintillation signal. In particular, the relative abundances of fast and slow components strongly depend on the particle type [7]. This property of LAr is crucial for discarding gamma and electron backgrounds from nuclear recoil events in direct dark matter search experiments ([5,8,35–37]).

The variable which is typically used to discriminate electron from nuclear recoils in LAr is F_{prompt}, which informs the abundance of the fast component in the scintillation signal and is defined as:

$$F_{\mathrm{prompt}} = \frac{\int_0^{t^*} l(t)dt}{\int_0^{\infty} l(t)dt} \tag{24}$$

where $l(t)$ is the scintillation waveform and t^* is the integration time of the fast component which maximizes the separation. Different values of t^* are used by different groups, but it is typically close to 100 nsec. F_{prompt} depends on the recoil energy and the separation between electron and nuclear recoils tends to get worse at lower energies. The proposed model contains explicitly the dependence of the scintillation signals of electron and nuclear recoils from the density of deposited energy and can be used to predict and explain the behavior of F_{prompt} observed experimentally.

In order to evaluate F_{prompt} for electrons as a function of the kinetic energy, E, of the incoming electron, $F^e_{\mathrm{prompt}}(E)$, it is necessary to evaluate the parameters k^+ and q of Eq. (7). The parameter k^+ is proportional to the number density N_0^+ of Ar_2^+, whose dependence on the density of deposited energy is not known. It is reasonable to assume, in first approximation, that it stays constant in the region of interest, below 1 MeV. The density of deposited energy varies very slowly down to 100 keV, where it starts increasing more steeply. In this low energy region the effect of the increased density is compensated by the reduction of the escaping probability for the ionization electrons due to the increased electric field in the core of the track.

The parameter q is equal to:

$$q^e = \sigma_3 v_3 N_0 = \sigma_3 v_3 \left[\frac{dE}{dx}\frac{1}{r_3^2}\right]\frac{\alpha_3^e}{W_{\rm el}}\left(1 - R(0) + \frac{N_{\rm ex}}{N_i}\right) \quad (25)$$

where dE/dx is the electronic stopping power of argon, $[dE/dx\, r_3^2]$ is the average value of the density of deposited energy along the track, $W_{\rm el} = 23.6$ eV is the average energy to produce an electron-ion pair in LAr [7], R(0) is the recombination factor at zero electric field and $\alpha_3^e = 0.86$ is the initial relative abundance of triplet states for electron recoils. For low energy electrons (<1 MeV), according to Bohr's theory [38], r_3 is proportional to $\gamma\beta$, in particular:

$$\frac{dE}{dx}\frac{1}{r_3^2} \simeq \frac{dE}{dx}\frac{\bar{\nu}^2}{c^2\beta^2\gamma^2} \quad (26)$$

where c is the speed of light, $\beta = v/c$, $\gamma = 1/\sqrt{(1-\beta^2)}$, and $\bar{\nu}$ is the average orbiting frequency of atomic electrons, which is related to the mean excitation energy, I, by the relation $I = h\bar{\nu}$. For argon, I = 188 eV. Using Eqs. (25) and (26), q is written as:

$$q^e(E) = k_q^e d^e(E) \quad (27)$$

where $d^e(E)$ is the average value along the track of the density of deposited energy of Eq. (26) multiplied by α_3^e:

$$d^e(E) = \int_0^E \frac{dE'}{dx}\frac{\alpha_3^e \bar{\nu}^2}{c^2\beta^2\gamma^2}\frac{dE'}{E} \quad (28)$$

and k_q^e is a characteristic constant:

$$k_q^e = \frac{\sigma_3 v_3}{W_{\rm el}}\left(1 - R(0) + \frac{N_{\rm ex}}{N_i}\right) \quad (29)$$

In order to compare the model to data, the integral of Eq. (28) is evaluated numerically using tabulated values for the electronic stopping power [39].

$d^e(E)$ is well fitted, for E < 1 MeV, by the analytical expression:

$$d^e(E) = 843(E^{-0.65} - 1.48E^{-0.43} + 0.66) \quad (30)$$

with E in MeV and d^e in MeV/μm^3. The model prediction is compared to experimental data from [8,37]. $F^e_{\rm prompt}$ is calculated as:

$$F^{e,n}_{\rm prompt} = \frac{p_1 L_s + p_2 L_3}{L_s + L_3} \quad (31)$$

where L_1 and L_3 are the abundances of the fast and slow components respectively [see Eq. (8)], the parameters p_1 and p_2 are related to the integration process for the calculation of $F^{e,n}_{\rm prompt}$ [see Eq. (24)] and in particular to the fraction of fast and slow component which fall inside the integration window. Typically p_1 is close to one and p_2 is close to zero. The fact of p_1 not being exactly equal to one is attributed to the delayed light emission of the wavelength shifters used to detect LAr photons [26]. The parameters p_1, p_2 and k_q^e are left free and adjusted on data. The two datasets have been fitted separately, since they show some differences in their asymptotic behaviors at large energies, which is probably related to different integration intervals, and in their slopes at low energies. The result of the fitting procedures is shown in Fig. 5. The values of $k_q^e = 0.73 \times 10^{-7}$ nsec^{-1} MeV^{-1} μm^3 for [8] and $k_q^e = 1.9 \times 10^{-7}$ nsec^{-1} MeV^{-1} μm^3 for [37] are obtained.

In the case of a low energy nuclear recoils of an argon atom in LAr, below few hundreds of keV, a significant amount of the energy lost by the recoiling argon atom is due to elastic collisions with other argon nuclei and only a small fraction of it is transferred to the electrons. The Lindhard theory [19,40] gives the amount of energy transferred to the electrons of the LAr in terms of the dimensionless variable ε:

$$\varepsilon = C_\varepsilon E = \frac{a_{TFF} A_2}{Z_1 Z_2 e^2 (A_1 + A_2)} E \quad (32)$$

where E is the recoil energy, Z and A are the atomic and mass number of the projectile (1) and of the medium (2) and:

$$a_{TFF} = \frac{0.8853 a_B}{(Z_1^{1/2} + Z_2^{1/2})^{2/3}} \quad (33)$$

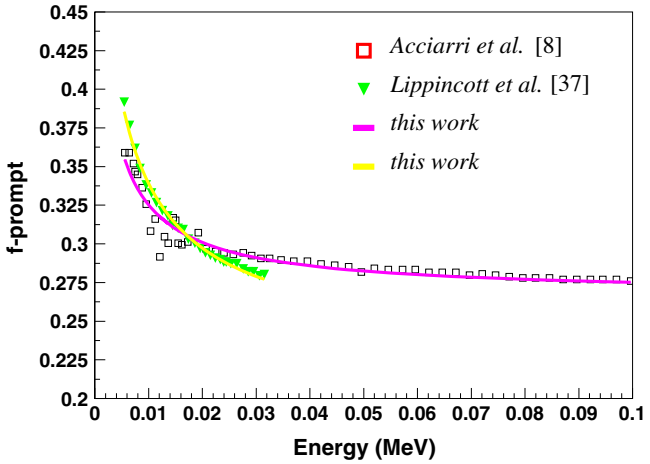

FIG. 5. $F_{\rm prompt}$ for low energy electrons in LAr measured by two experimental groups [8,37]. The experimental points have been fitted with Eq. (31) with fitting parameters p_1, p_2 and k_q (see text). The results of the fit procedures are shown with magenta ([8]) and green ([37]) lines.

$a_B = \hbar/m_e e^2 = 0.529$ Å is the Bohr radius. For $Z_1 = Z_2$ equation (32) gives $C_\varepsilon = 0.01354$ keV^{-1}. The amount of energy transferred to the electrons is given by [22]:

$$\eta(\varepsilon) = \frac{k\, g(\varepsilon)\, \varepsilon}{1 + k\, g(\varepsilon)} \tag{34}$$

where $k = 0.133 Z^{2/3} A^{-1/2} = 0.144$ and g(ε) is fitted with the function [22]:

$$g(\varepsilon) = 3\varepsilon^{0.15} + 0.7\varepsilon^{0.6} + \varepsilon \tag{35}$$

Low energy nuclear recoils deposit their energy in a very confined portion of space. The projected range for argon ions of tens of keV kinetic energy in LAr is of the order of few hundreds of Å [41] and the transversal dimensions of the core of the track is of the order of the Bohr radius a_B [19]. It is reasonable to assume that in this range of energies, the spatial distribution of the Ar_2^* is largely dominated by the fast diffusion of excitons and holes before self-trapping and by the coulombian repulsion of the Ar ions in the core of the track. Under this hypothesis, the recoil energy is deposited inside an approximately constant volume at very low energies. A linear growth of this volume with energy is expected, since the total stopping power is constant for energies below few hundreds of keV [19,40] and the range of the Ar ions is proportional to its initial kinetic energy, while the transversal dimensions continue being dominated by fast diffusive processes. Using Eqs. (25) and (34), the factor q for low energy nuclear recoils is written as:

$$q^n(E) = k_q^n\, d^n(E) = k_q^n \frac{\alpha_3^n}{V_0} \frac{\eta(E)}{1 + k_V E} \tag{36}$$

where $\alpha_3^n = 0.36$ is the initial relative abundance of triplet states for nuclear recoils, V_0 is the volume inside which the energy deposited by nuclear recoils is contained for very low energies, k_V takes into account the increase of the volume with the recoil energy and k_q^n is given by:

$$k_q^n = \frac{\sigma_3 v_3}{W_{\rm el}} \left(1 + \frac{N_{\rm ex}}{N_i}\right) \tag{37}$$

Equations (36) and (8) (with $\tau_q = \tau_3$) can be substituted in Eq. (31) to evaluate $F^n_{\rm prompt}$ for nuclear recoils and compare it to available data.

The model is fitted to the data reported in [8] and referred to, as the *high light yield* sample, which span a broad interval of energies, from 10 keV to above 1 MeV.

The conversion between the number of detected photoelectrons ($N_{\rm phel}$) and the nuclear recoil energy in [8] is done assuming a constant relative scintillation yield between nuclear and electron recoils, $\mathcal{L}_{\rm eff}$, equal to 0.3. A more appropriate conversion between $N_{\rm phel}$ and the recoil energy, E_n, is given by:

$$E_n = \frac{N_{\rm phel}}{LY \times \mathcal{L}_{\rm eff}(E_n)} \tag{38}$$

where LY is the light yield for electron recoils expressed in phel/keV. The fit procedure of the $F^n_{\rm prompt}$ data reported in [8], which takes into account Eq. (38) is described in the following section.

VII. QUENCHING FACTOR FOR NUCLEAR RECOILS

The quenching of the number of emitted photons in a nuclear recoil event is described as the succession of three distinct quenching processes: (i) the quenching of the amount of energy transferred to the atomic electrons (Q^L), due to the elastic collisions of the argon ion with surrounding argon atoms [40]; (ii) the quenching of the excitons formed after the nuclear recoil (Q^E), due to biexcitonic quenching [19]; (iii) the quenching of the triplet states formed after the trapping of the excitons (Q^T), due to triplet-triplet interactions (and triplet-ion in the presence of Ar_2^+). The overall quenching factor for nuclear recoils can be written as:

$$Q^N = Q^L \times Q^E \times Q^T \tag{39}$$

Q_L is the quenching factor of process (i), which has been calculated by Lindhard [40] and can be written as [refer to Eq. (34)]:

$$Q^L = \frac{\eta(\varepsilon)}{\varepsilon} = \frac{k\, g(\varepsilon)}{1 + k\, g(\varepsilon)} \tag{40}$$

Q^E is the quenching factor of process (ii). It has been pointed out in [18] that Q^E can be considered approximately constant for energies below few hundreds of keV. This approximation has been proven to work well for liquid xenon [42]. Q^T is the quenching factor for process (iii), discussed in this work. It can be written as [see Eq. (8)]:

$$Q^T = \alpha_s + \alpha_3 \frac{\ln(1 + q^n(E)\tau_3)}{q^n(E)\tau_3} \tag{41}$$

where $\alpha_s = 0.64$, $\alpha_3 = 0.36$, $\tau_3 = 2100$ nsec and $q^n(E)$ is given by Eq. (36).

Experimentally, it is convenient to measure the relative scintillation yield of nuclear recoils with respect to electron recoils, $\mathcal{L}_{\rm eff}$. Nuclear recoils are typically compared to the recoils of electrons emitted after the photoabsorption of the γ lines of ^{241}Am (59.5 keV) and ^{57}Co (122 keV). $\mathcal{L}_{\rm eff}$ can be estimated as:

$$\mathcal{L}_{\rm eff} = \frac{Q^N}{Q^{\rm el}} = Q^L \times Q^T \times \frac{Q^E}{Q^{\rm el}} \tag{42}$$

where $Q^{\rm el}$ is the quenching factor of the reference electron recoil. Since Q^E and $Q^{\rm el}$ are both constant, the ratio $Q^E/Q^{\rm el}$ is an overall multiplicative constant in Eq. (42).

In order to estimate the parameters of the model, an overall fit of the $F^n_{\rm prompt}$ data from [8] and of the $\mathcal{L}_{\rm eff}$ data reported by the ARIS (Argon Response to Ionization and Scintillation) Collaboration in [43] is performed, where the product $k^n_q\alpha^n_3/V_0$ and k_V from Eq. (36) and the ratio $Q^E/Q^{\rm el}$ of Eq. (42) are left as free parameters. The exact value of E_n for the $F^n_{\rm prompt}$ set of data is obtained by inverting numerically Eq. (38). The fit procedure returns a value of 0.11 ± 0.01 MeV^{-1} nsec^{-1} for the product $k^n_q\alpha^n_3/V_0$, 9.1 ± 0.1 Mev^{-1} for k_V and 1.00 ± 0.01 for the ratio $Q^E/Q^{\rm el}$. Taking into account the value of k^e_q found with the fit of $F^e_{\rm propmpt}$ for electron recoils, that $\alpha^n_3 = 0.36$ and that the recombination factor for nuclear recoils at zero electric field is zero ($\mathrm{R}(0) = 0$), the volume V_0 ranges between 200 and 500 nm^3. This corresponds to a sphere with a diameter between 7 and 10 nm, which is in a reasonable agreement with the diffusion of free excitons and holes before trapping, for times of the order of 1 ps and assuming a diffusion constant $\mathrm{D} = 1$ cm^2/sec [19].

A fit procedure which uses only the $F^n_{\rm prompt}$ dataset is able to constrain pretty well the terms $k^n_q\alpha^n_3/V_0$ and k_V, giving results compatible with the ones reported here, while the range for the ratio $Q^E/Q^{\rm el}$ turns out to be quite broad (between 0.9 and 1.1). The same ratio $Q^E/Q^{\rm el}$ could be estimated following the α-core approximation discussed in [19] giving a value close to unity, but with a quite large uncertainty (at the level of 20%–30%).

The result of the fit for $F^n_{\rm prompt}$ is shown in Fig. 6 together with three more datasets. The dataset referred as *low light yield* is also taken from [8], but it is obtained with a different experimental setup, with a lower light yield with respect to the *high light yield* one. The two other datasets are taken from [35,37].

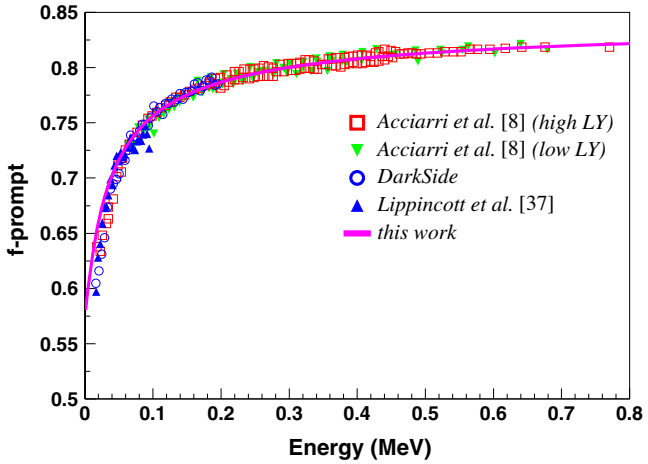

FIG. 6. $F_{\rm prompt}$ for nuclear recoils in LAr measured by different authors [8,35,37]. The high light yield sample (see text) from [8] is used to fit the data. Magenta line represents the fit result. The datasets have been aligned by applying overall scale factors which vary between 1.01 and 1.05.

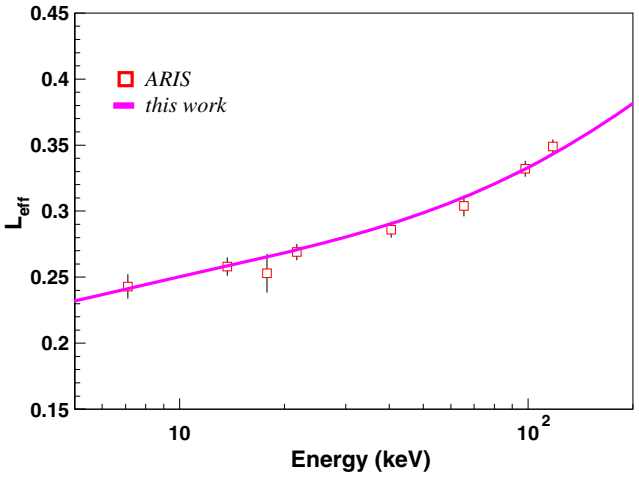

FIG. 7. Comparison of the model prediction for $\mathcal{L}_{\rm eff}$ (magenta line) with the data from the ARIS Collaboration [43] (see text).

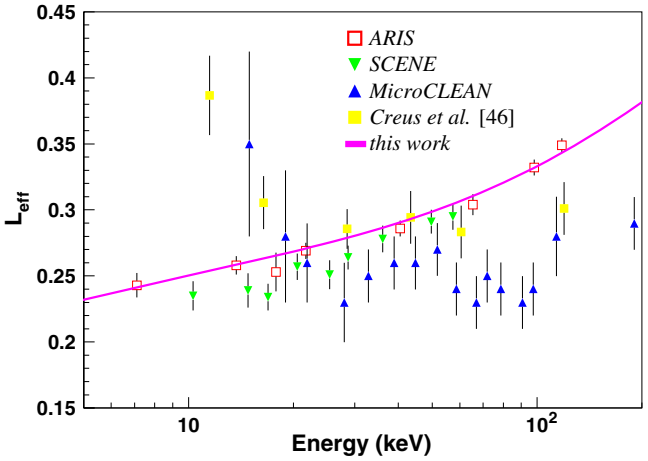

FIG. 8. Comparison of the model prediction for $\mathcal{L}_{\rm eff}$ (magenta line) with data taken from [43–46].

The datasets have been aligned by applying overall scaling factors to the $F^n_{\rm prompt}$ values (one per each dataset), which range between 1.01 and 1.05. The not perfect overlap of the different datasets before rescaling is attributed to different integration intervals to compute $F^n_{\rm prompt}$ and to small systematic effects.

The result of the fit for $\mathcal{L}_{\rm eff}$ is shown in Fig. 7. The model prediction, together with the majority of available data is shown in Fig. 8.

VIII. DISCUSSION

The triplet-triplet quenching reaction 1 has enough energy to ionize one of the two interacting triplet states, since the band gap of LAr is about 14.2 eV [47]. The model

assumes that the ionized molecule and the electron recombine in a triplet state. This is a good assumption if the spin relaxation time of the ion-electron system is long compared to the recombination time. The possibility that the ion-electron system recombines in a singlet state has been tested by explicitly including it in the model and a very small contribution, at the level of percent, has been found and it has been neglected.

The triplet-ion quenching reaction 2 has enough energy to dissociate the Ar_2^+ ion, whose binding energy is about 1.3 eV [48], and the model assumes that the Ar^+ and Ar recombine and the density of Ar_2^+ states does not change. An important hypothesis of the model is to neglect the diffusion terms in Eqs. (3) and (4). In the case of low LET particles this is well justified by the transversal distribution (with respect to particle direction) of the density of deposited energy which is grater than hundreds of nm, while the diffusion constant of Ar_2^* should be of the order of 10^{-6} cm^2/s or less [49]. This assumption is also consistent with the results obtained for nuclear recoils, since the volume inside which the electronic excitation energy is found to be released is compatible with the simple diffusion of free excitons and holes before self-trapping (see Sec. VII) and the contribution of Ar_2^* diffusion should be negligible on the timescale of LAr scintillation emission.

The model introduces a possible additional quenching mechanism of the scintillation light in LAr and poses a serious question about its absolute photon yield. This does not necessarily means that the photon yield (after the quenching) is different from what is widely assumed, since it has never been directly measured. It is believed that the ideal photon yield (51,000 photons/MeV [50]), estimated on the basis of the value of W_{el} and N_{ex}/N_i, is reached by relativistic heavy ions and then scaled for the other particles and energies according to the experimental results of relative measurements. This point should be experimentally addressed since the technology of light detection is mature enough to allow precision measurements of the photon yield. This and other measurements and characterizations of the LAr scintillation light properties would be extremely desirable in view of the design of the next generation experiments for neutrino and dark matter direct detection.

IX. CONCLUSIONS

This work describes a model for the production of LAr scintillation light which takes into account the quenching of Ar_2^* through self interactions and interactions with Ar_2^+ ions. It allows to justify two processes which could not be explained otherwise: the dependence of the slow scintillation decay time from the intensity of an external electric field and the increase of the photon yield of xenon doped liquid argon, both for low LET particle interactions. It is possible to make an accurate prediction of the time profile of the scintillation pulse where the dependence on the electric field and on the density of the deposited energy is explicit. A simultaneous fit to experimental average waveforms of electron and nuclear recoil events allows to constrains some of the most relevant parameters of the model such as the unquenched decay time of the slow scintillation component, τ_3, which results to be around 2100 nsec and the relative abundance of singlet and triplet states for electron and nuclear recoils.

Knowing the shape of the scintillation pulse makes it possible to analytically calculate the relative abundance of the fast component, F_{prompt}, which is often used as a pulse shape discrimination parameter. The expressions of F_{prompt} for electron and nuclear recoils need to be fitted to the available data to extract some of the parameters which are not precisely known, but the overall behavior is well reproduced.

The model allows to predict the shape of the relative scintillation efficiency for nuclear recoils in LAr, $\mathcal{L}_{eff}$, and it has been shown that it reproduces closely the experimental data reported by the ARIS Collaboration [43].

LAr is a powerful medium for particle detection which is being widely used in many fields of fundamental particle physics. Deepening the knowledge of its properties can greatly benefit the design of the next generation of detectors.

ACKNOWLEDGMENTS

This work was supported by FAPESP (Fundação de Amparo à Pesquisa do Estado de São Paulo) with the Grant No. 2016/01106-5 and by CNPq (Conselho Nacional de Desenvolvimento Científico e Tecnológico with the Grant No. 305240/2019-6. The author thanks the members of the *HdM* team, which is still, virtually, alive: Flavio Cavanna, Nicola Canci, Roberto Acciarri, and Andrzej Szelc and which is the source of some of the data used in this work. The author warmly thanks Ana Machado for her suggestions and for the continuous discussions which helped the analyses presented here and Paola Tomassini who inspired and guided this work since the beginning.

[1] DUNE-Collaboration, Volume I. Introduction to DUNE, J. Instrum. **15**, T08008 (2020).

[2] C. Rubbia *et al.*, Underground operation of the ICARUS t600 LAr-TPC: First results, J. Instrum. **6**, P07011 (2011).

[3] H. Chen *et al.* (MicroBooNE Collaboration), Proposal for a new experiment using the booster and NuMI neutrino beamlines: MicroBooNE (2007), https://inspirehep.net/literature/776376.

[4] P. A. Machado, O. Palamara, and D. W. Schmitz, The short-baseline neutrino program at fermilab, Annu. Rev. Nucl. Part. Sci. **69**, 363 (2019).

[5] R. Acciarri, M. Antonello, B. Baibussinov, P. Benetti, F. Calaprice, E. Calligarich, M. Cambiaghi, N. Canci, C. Cao, F. Carbonara, F. Cavanna, S. Centro, M. Ceolin, A. Chavarria, A. Cocco, F. Di Pompeo, G. Fiorillo, C. Galbiati, L. Grandi, and C. Vignoli, The warp experiment, J. Phys. Conf. Ser. **203**, 012006 (2010).

[6] P. Agnes *et al.*, First results from the darkside-50 dark matter experiment at laboratori nazionali del gran sasso, Phys. Lett. B **743**, 456 (2015).

[7] T. Doke, Fundamental properties of liquid argon, krypton and xenon as radiation detector media, Portugaliae Physica **12**, 9 (1981).

[8] R. Acciarri, N. Canci, F. Cavanna, P. Kryczynski, L. Pandola, E. Segreto, and A. Szelc, Neutron to gamma pulse shape discrimination in liquid argon detectors with high quantum efficiency photomultiplier tubes, Phys. Procedia **37**, 1113 (2012).

[9] C. G. Wahl, E. P. Bernard, W. H. Lippincott, J. A. Nikkel, Y. Shin, and D. N. McKinsey, Pulse-shape discrimination and energy resolution of a liquid-argon scintillator with xenon doping, J. Instrum. **9**, P06013 (2014).

[10] S. Amoruso *et al.*, Analysis of the liquid argon purity in the icarus t600 tpc, Nucl. Instrum. Methods Phys. Res., Sect. A **516**, 68 (2004).

[11] DUNE-Collaboration, Volume IV. The DUNE far detector single-phase technology, J. Instrum. **15**, T08010 (2020).

[12] A. Badertscher, F. Bay, N. Bourgeois, C. Cantini, M. Daniel, U. Degunda, S. DiLuise, L. Epprecht, A. Gendotti, S. Horikawa, L. Knecht, D. Lussi, G. Maire, B. Montes, S. Murphy, G. Natterer, K. Nikolics, K. Nguyen, L. Periale, S. Ravat, F. Resnati, L. Romero, A. Rubbia, R. Santorelli, F. Sergiampietri, D. Sgalaberna, T. Viant, and S. Wu (A. Collaboration), Status of the ARDM experiment: First results from gaseous argon operation in deep underground environment, arXiv:1307.0117.

[13] A. Hime, The miniclean dark matter experiment, arXiv:1110.1005.

[14] M. G. Boulay and DEAP Collaboration, DEAP-3600 dark matter search at SNOLAB, J. Phys. Conf. Ser. **375**, 012027 (2012).

[15] P. Benetti, R. Acciarri, F. Adamo, B. Baibussinov, M. Baldoceolin, M. Belluco, F. Calaprice, E. Calligarich, M. Cambiaghi, and F. Carbonara *et al.*, First results from a dark matter search with liquid argon at 87k in the Gran Sasso underground laboratory, Astropart. Phys. **28**, 495 (2008).

[16] V. Zacek, Dark matter, Fundam. Interact., 170 (2007).

[17] C. E. Aalseth, F. Acerbi, P. Agnes, I. F. M. Albuquerque, T. Alexander, A. Alici, A. K. Alton, P. Antonioli, S. Arcelli, R. Ardito *et al.*, Darkside-20k: A 20 tonne two-phase lar tpc for direct dark matter detection at LNGS, Eur. Phys. J. Plus **133**, 131 (2018).

[18] A. Hitachi, T. Doke, and A. Mozumder, Luminescence quenching in liquid argon under charged-particle impact: Relative scintillation yield at different linear energy transfers, Phys. Rev. B **46**, 11463 (1992).

[19] A. Hitachi and A. Mozumder, Properties for liquid argon scintillation for dark matter searches, arXiv:1903.05815.

[20] M. Miyajima, T. Takahashi, S. Konno, T. Hamada, S. Kubota, H. Shibamura, and T. Doke, Average energy expended per ion pair in liquid argon, Phys. Rev. A **9**, 1438 (1974).

[21] T. Doke, H. J. Crawford, C. R. Gruhn, A. Hitachi, J. Kikuchi, K. Masuda, S. Nagamiya, E. Shibamura, and S. Tamada, Scintillation yields by relativistic heavy ions and the relation between ionization and scintillation in liquid argon, Nucl. Instrum. Methods Phys. Res., Sect. A **235**, 136 (1985).

[22] D. M. Mei, Z.-B. Yin, L. C. Stonehill, and A. Hime, A model of nuclear recoil scintillation efficiency in noble liquids, Astropart. Phys. **30**, 12 (2008).

[23] J. B. Birks, Scintillations from organic crystals: Specific fluorescence and relative response to different radiations, Proc. Phys. Soc. London Sect. A **64**, 874 (1951).

[24] C. Lastoria (DUNE Collaboration), Analysis of the light production and propagation in the 4-tonne dual-phase demonstrator, J. Instrum. **15**, C06029 (2019).

[25] B. Aimard, C. Alt, J. Asaadi, M. Auger, V. Aushev, D. Autiero, M. Badoi, A. Balaceanu, G. Balik, L. Balleyguier *et al.*, A 4 tonne demonstrator for large-scale dual-phase liquid argon time projection chambers, J. Instrum. **13**, P11003 (2018).

[26] E. Segreto, Evidence of delayed light emission of tetraphenyl-butadiene excited by liquid-argon scintillation light, Phys. Rev. C **91**, 035503 (2015).

[27] C. Benson, G. O. Gann, and V. Gehman, Measurements of the intrinsic quantum efficiency and absorption length of tetraphenyl butadiene thin films in the vacuum ultraviolet regime, Eur. Phys. J. C **78**, 329 (2018).

[28] R. Acciarri, Measurement of the scintillation time spectra and pulse shape discrimination of low-energy electron and nuclear recoils in liquid argon with the warp 2.3 lt detector, Ph.D. thesis, University of L'Aquila, 2010.

[29] R. Francini, R. M. Montereali, E. Nichelatti, M. A. Vincenti, N. Canci, E. Segreto, F. Cavanna, F. D. Pompeo, F. Carbonara, G. Fiorillo, and F. Perfetto, Tetraphenyl-butadiene films: VUV-vis optical characterization from room to liquid argon temperature, J. Instrum. **8**, P09006 (2013).

[30] S. Amoruso *et al.*, Study of electron recombination in liquid argon with the icarus tpc, Nucl. Instrum. Methods Phys. Res., Sect. A **523**, 275 (2004).

[31] C. Benson, G. O. Gann, and V. Gehman, Measurements of the intrinsic quantum efficiency and absorption length of tetraphenyl butadiene thin films in the vacuum ultraviolet regime, Eur. Phys. J. C **78**, 329 (2018).

[32] S. Kubota, M. Hishida, S. Himi, J. Suzuki, and J. Ruan, The suppression of the slow component in xenon-doped liquid argon scintillation, Nucl. Instrum. Methods Phys. Res., Sect. A **327**, 71 (1993).

[33] Xe_2^* singlet and triplet states are treated together here, since their decay times are very close [34].
[34] T. Doke and K. Masuda, Present status of liquid rare gas scintillation detectors and their new application to gamma-ray calorimeters, Nucl. Instrum. Methods Phys. Res., Sect. A **420**, 62 (1999).
[35] P. Agnes *et al.* (DarkSide Collaboration), Results from the first use of low radioactivity argon in a dark matter search, Phys. Rev. D **93**, 081101 (2016).
[36] C. Regenfus, The argon dark matter experiment, in *Proceedings of the 4th Patras Workshop on Axions, WIMPs and WISPs, PATRAS 2008* (DESY, Hamburg, 2009), Vol. 203.
[37] W. H. Lippincott, K. J. Coakley, D. Gastler, A. Hime, E. Kearns, D. N. McKinsey, J. A. Nikkel, and L. C. Stonehill, Scintillation time dependence and pulse shape discrimination in liquid argon, Phys. Rev. C **78**, 035801 (2008).
[38] W. Leo, *Techniques for Nuclear and Particle Physics Experiments: A How to Approach* (Springer, Berlin, 1987).
[39] M. J. Berger, J. S. Coursey, M. A. Zucker, and J. Chang ESTAR, PSTAR, and ASTAR: Computer Programs for Calculating Stopping-Power and Range Tables for Electrons, Protons, and Helium Ions (version 1.2.3) (2005).
[40] J. Lindhard, V. Nielsen, M. Scharff, and P. V. Thomsen, Integral equations governing radiation effects (notes on atomic collisions, iii), Kgl. Danske Videnskab., Selskab. Mat. Fys. Medd, Vol. **33**.
[41] J. F. Ziegler, M. Ziegler, and J. Biersack, Srim the stopping and range of ions in matter, Nucl. Instrum. Methods Phys. Res., Sect. B **268**, 1818 (2010).
[42] A. Hitachi, Properties of liquid xenon scintillation for dark matter searches, Astropart. Phys. **24**, 247 (2005).
[43] P. Agnes, J. Dawson, S. De Cecco, A. Fan, G. Fiorillo, D. Franco, C. Galbiati, C. Giganti, T. N. Johnson, G. Korga, D. Kryn, M. Lebois, A. Mandarano, C. J. Martoff, A. Navrer-Agasson, E. Pantic, L. Qi, A. Razeto, A. L. Renshaw, Q. Riffard, B. Rossi, C. Savarese, B. Schlitzer, Y. Suvorov, A. Tonazzo, H. Wang, Y. Wang, A. W. Watson, and J. N. Wilson (The ARIS Collaboration), Measurement of the liquid argon energy response to nuclear and electronic recoils, Phys. Rev. D **97**, 112005 (2018).
[44] H. Cao *et al.* (SCENE Collaboration), Measurement of scintillation and ionization yield and scintillation pulse shape from nuclear recoils in liquid argon, Phys. Rev. D **91**, 092007 (2015).
[45] D. Gastler, E. Kearns, A. Hime, L. C. Stonehill, S. Seibert, J. Klein, W. H. Lippincott, D. N. McKinsey, and J. A. Nikkel, Measurement of scintillation efficiency for nuclear recoils in liquid argon, Phys. Rev. C **85**, 065811 (2012).
[46] W. Creus, Y. Allkofer, C. Amsler, A. Ferella, J. Rochet, L. Scotto-Lavina, and M. Walter, Scintillation efficiency of liquid argon in low energy neutron-argon scattering, J. Instrum. **10**, P08002 (2015).
[47] V. Chepel and H. Araújo, Liquid noble gas detectors for low energy particle physics, J. Instrum. **8**, R04001 (2013).
[48] K.-M. Weitzel and J. Mhnert, The binding energies of small Ar, CO AND N2 cluster ions, Int. J. Mass Spectrom. **214**, 175 (2002).
[49] G. CiniCastagnoli and F. P. Ricci, Selfdiffusion in liquid argon, J. Chem. Phys. **32**, 19 (1960).
[50] T. Doke, K. Masuda, and E. Shibamura, Estimation of absolute photon yields in liquid argon and xenon for relativistic (1 MeV) electrons, Nucl. Instrum. Methods Phys. Res., Sect. A **291**, 617 (1990).